Published in final edited form as:
*Bone*. 2011 November ; 49(5): 923–930. doi:10.1016/j.bone.2011.07.013.

# Surface Contaminants Inhibit Osseointegration in a Novel Murine Model

**Lindsay A. Bonsignore**[a,b], **Robb W. Colbrunn**[e], **Joscelyn M. Tatro**[a], **Patrick J. Messerschmitt**[a], **Christopher J. Hernandez**[c], **Victor M. Goldberg**[a], **Matthew C. Stewart**[f], and **Edward M. Greenfield**[a,b,d]

[a]Department of Orthopaedics, Case Western Reserve University, Cleveland, Ohio

[b]Department of Pathology, Case Western Reserve University, Cleveland, Ohio

[c]Department of Mechanical and Aerospace Engineering, Case Western Reserve University, Cleveland, Ohio

[d]National Center for Regenerative Medicine, Case Western Reserve University, Cleveland, Ohio

[e]Department of Biomedical Engineering, Cleveland Clinic, Cleveland, Ohio

[f]College of Veterinary Medicine, University of Illinois, Urbana-Champaign, IL

## Abstract

Surface contaminants, such as bacterial debris and manufacturing residues, may remain on orthopaedic implants after sterilization procedures and affect osseointegration. The goals of this study were to develop a murine model of osseointegration in order to determine whether removing surface contaminants enhances osseointegration. To develop the murine model, titanium alloy implants were implanted into a unicortical pilot hole in the mid-diaphysis of the femur and osseointegration was measured over a five week time course. Histology, backscatter scanning electron microscopy and x-ray energy dispersive spectroscopy showed areas of bone in intimate physical contact with the implant, confirming osseointegration. Histomorphometric quantification of bone-to-implant contact and peri-implant bone and biomechanical pullout quantification of ultimate force, stiffness and work to failure increased significantly over time, also demonstrating successful osseointegration. We also found that a rigorous cleaning procedure significantly enhances bone-to-implant contact and biomechanical pullout measures by two-fold compared with implants that were autoclaved, as recommended by the manufacturer. The most likely interpretation of these results is that surface contaminants inhibit osseointegration. The results of this study justify the need for the development of better detection and removal techniques for contaminants on orthopaedic implants and other medical devices.

### Keywords

contaminants; osseointegration; murine; histomorphometry; biomechanical testing



**Corresponding Author**: Edward Greenfield, PhD, Department of Orthopaedics, Case Western Reserve University, 2109 Adelbert Road, Biomedical Research Building Room 331, Cleveland, OH 44106, Phone# 1-216-368-1331, Fax# 1-216-368-1332, edward.greenfield@case.edu.

## 1. Introduction

There are over 600,000 total joint arthroplasties performed each year in the United States [1]. The demand for total joint arthroplasty will continue to rise and is expected to exceed 4 million per year in the United States by 2030 [1]. Although, total joint arthroplasty provides excellent 10–15 year outcomes, aseptic loosening of cementless implants remains a major clinical problem [2,3]. Revision arthroplasty has a higher complication rate, is more difficult, and is more costly than primary procedures [2]. Patients below age 65 now represent 35–45% of all total joint arthroplasty recipients in the United States [4,5]. These patients will most likely outlive the lifespan of current joint arthroplasties and many of them will require a revision surgery.

Clinical success of a cementless total joint arthroplasty depends upon two main factors: initial fixation due to osseointegration in the first few months after surgery and maintenance of the fixation over the long term [6]. Osseointegration provides a biomechanically stable environment in which the implant can persist under conditions of normal loading [7,8]. The initial events necessary for osseointegration include mesenchymal cell attachment, spreading, proliferation and differentiation into matrix-secreting osteoblasts on the implant surface that results in the formation of mineralized bone around the implant [9].

Impaired osseointegration is a clinically significant problem, especially in patients with osteoporosis [10], diabetes [11], immunosuppressive therapy [12], smoking [13,14], revision surgeries [15,16] and other conditions with reduced bone formation. Increased early motion between the implant and the bone also has a detrimental effect on osseointegration [17]. This impaired osseointegration leads to an increased risk of subsequent loosening due to micromotion [18] and/or wear particle migration along the implant which can enhance particle-mediated osteolysis [19].

Many prior studies of osseointegration have focused on the effects of differing implant compositions [20,21], surface topographies [22,23,24,25], and adsorption of adhesion proteins [26,27,28]. In contrast, few studies have focused on surface contaminants that may inhibit osseointegration. More rigorous cleaning procedures are generally required to remove these contaminants than to achieve sterility [29]. For example, bacterial debris and manufacturing residues can remain on an implant surface after sterilization procedures such as autoclaving. The best characterized bacterial debris, lipolysaccharide (LPS), is derived from Gram-negative bacteria and is resistant to extreme temperatures and pH values [30,31]. LPS is ubiquitous and has a high affinity for biomaterial surfaces [30,32,33]. It induces inflammatory pathophysiological responses by activating Toll-Like Receptor 4 (TLR-4), which is expressed by most mammalian cell types [34]. Other common bacterial-derived debris that induce similar inflammatory effects include lipoteichoic acids from Gram-positive bacteria and lipopeptides and peptidoglycans derived from both Gram-positive and Gram-negative bacteria [35]. The US Food and Drug Administration (FDA) requires manufacturers to test for LPS by immersing medical devices in water and then measuring the eluted LPS [36]. However, water elution of adherent LPS from a biomaterial is inefficient [30,32,33]. Considerable amounts of LPS and other bacterial debris may therefore adhere to the surface of an implant despite low levels of LPS in the eluate.

Non-biological contaminants can also exist on sterilized implants. These contaminants include heavy metals, grit blast material, oil residues, lubricants, cleaning agents, processing aids, handling equipment and packaging debris that can be introduced onto the surface during manufacturing processes [29,37,38]. In the last seven years, the FDA has recalled 26 medical devices due to process contamination [39]. For example, a specific lot of hip replacement acetabular cups that was associated with impaired osseointegration and early

failure rates was found to be contaminated with both LPS and oil residues [40]. FDA regulatory guidelines for medical devices stipulate that manufacturers identify possible residues, establish a residue limit, to stay below that limit, and to document and validate cleanliness as part of an ongoing process [38]. However, the FDA guidelines do not specify contamination limits or appropriate analytic techniques.

Contaminants that remain on sterilized medical devices, such as orthopaedic implants, may have pathophysiological effects in the body and affect the function of the device. To test this hypothesis, we developed a novel murine model of osseointegration and determined whether integration is enhanced by a rigorous cleaning procedure that our laboratory has previously shown removes greater than 99.9% of adherent LPS from titanium particles [30]. The novel murine model of osseointegration is based on a previous established rat model [41,42]. Titanium alloy implants, used clinically for craniofacial surgery, were implanted into a unicortical pilot hole in the mid-diaphysis of the femur. Osseointegration was then measured over a 5 week time course by histomorphometry and biomechanical pullout testing. Using this new model, we found that osseointegration is inhibited by contaminants that are removed by the rigorous cleaning procedure but not by routine autoclaving as recommended by the manufacturer. The results of this study provide rationale for the development of better detection and removal techniques for contaminants on orthopaedic implants.

## 2. Materials and Methods

### 2.1 Animals

The experimental protocol was approved by the Case Western Reserve University School of Medicine Institutional Animal Care and Use Committee. Male C57BL/6J mice (Jackson Laboratories, Bar Harbor, ME) were maintained at the Animal Resource Center of Case Western Reserve University. Animals were fed irradiated ProLab IsoPro RMH 3000 5p76 (PMI Nutritional International, St. Louis, MO) and water ad libitum.

### 2.2 Implants

Titanium alloy screws (KLS Martin, Jacksonville, FL), used clinically for craniofacial surgery, were utilized as implants. Screw shaped implants are centre-drive, self-tapping and measure 1 mm in diameter and 2 mm in length (Supplementary Figure 1A). Implants were autoclaved at 273°C for 8 minutes followed by a 30 minute dry cycle, as recommended by the manufacturer. Following autoclaving, a group of implants were rigorously cleaned with five alternating treatments of alkali ethanol (0.1 N NaOH and 95% ethanol at 32°C) and 25% nitric acid as we have previously described [30]. As a measure of adherent bacterial debris, implants from each group was assayed for adherent LPS using the Limulus Amebocyte Lysate (LAL) Assay (Lonza, Basel, Switzerland) with the addition of β-glucan blocker to prevent false positives due to β-glucan-like molecules [43]. Levels of adherent LPS are reported in Endotoxin Units (EU) per $m^2$ of surface area as determined in Section 2.4.3.

### 2.3 Surgical Procedure

Six to seven week old C57BL/6 male mice were randomly assigned to various groups and anesthetized with an intraperitoneal injection of a 60 ug Acepromazine, 1.7 mg Ketamine and 340 ug Xylazine. The right leg was shaved and scrubbed with betadine. An anterior 2 cm incision was made proximal to the patella and continued along the femur. The femur was exposed, without cutting the muscles, by dissecting between the rectus femoris and the vastus medialis muscles. A unicortical pilot hole was manually made in the anterior mid-diaphysis of the femur using a pilot hole drill (0.75 mm diameter, KLS Martin, Jacksonville, FL) and the implant was inserted. Implant placement was performed with limited exposure

to minimize soft tissue damage. The muscles were allowed to return to their original position and the incision was closed with sutures. Following surgery mice were allowed to ambulate freely. The mice tolerated the surgery well and were able to ambulate immediately but favored the operated leg for 1–2 days after surgery. The femur was inadvertently fractured during implant insertion in less than 5% of the mice and these mice were immediately sacrificed. Mice were sacrificed at 1 to 5 weeks following implantation for histological, μCT, or biomechanical evaluation.

## 2.4 Qualitative Analysis

**2.4.1 Histology—**Histological preparation was performed in the Case Western Reserve University Department of Orthopaedic's Hard Tissue Histology Core Facility. The femurs were dissected at the time of sacrifice and fixed in 10% formalin for 48 hours. After fixation, specimens were progressively dehydrated in ethanol and embedded in polymethyl-methacrylate (PMMA). Specimens were sectioned at a thickness of 200 μm using a low speed IsoMet saw with a diamond wafering blade (Buehler, Lake Bluff, IL), followed by polishing to approximately 100 μm (EchoMet, Buehler, Lake Bluff, IL). Because of the small size of the implant, it was only possible to obtain one central section of the implant per mouse. Sections were stained with Toluidine Blue (Fisher Scientific, Hampton, NH) with or without acid etching (0.2% formic acid). Alternatively, sections were stained with Sanderson's Rapid Bone Stain (Surgipath Medical Industries, Richmond, IL) with an acid fuchsin counterstain [44,45]. Contralateral femurs were also similarly sectioned and stained.

**2.4.2 Backscatter Scanning Electron Microscopy—**Backscatter scanning electron microscopy and x-ray energy dispersive spectroscopy were performed in the Swagelok Center for Surface Analysis of Materials at Case Western Reserve University. Specimens were progressively dehydrated in ethanol and 200 μm sections were prepared as in section 2.4.1. Unpolished and unstained sections were sputter-coated with gold for 2 minutes with the Denton Desk IV (Denton Vacuum, LLC, Moorestown, NJ). Sections were mounted using double-sided carbon tape to ensure grounding and then viewed using the type xT Nova Nanolab 200 (FEI, Hillsboro, OR) with a Nordlys II electron backscatter diffraction detector (Oxford Instruments, Oxfordshire, UK). Elemental analysis was performed by x-ray energy dispersive spectroscopy using the XFlash 4010 detector (Bruker AXS, Madison, WI) on the Nova Nanolab scanning electron microscope.

**2.4.3 μCT—**Specimens were fixed (see section 2.4.1) and μCT analysis was performed in the Cleveland Clinic Foundation Image Processing and Analysis Core using the eXplore Locus (GE Healthcare, Waukesha, WI) at a resolution of 20 μm. Surface area of the implants was determined from the μCT scans by generating an isosurface (Microview Software 2.1.2, GE Healthcare, Waukesha, WI)

## 2.5 Quantitative Analysis

**2.5.1 Histomorphometric Analysis—**Bone-to-implant contact (BIC) and peri-implant bone were measured by a blinded observer in cross-sections (100X, Leica DMIRB, Wetzlar, Germany) using ImageJ analysis software. The percentage of BIC was calculated in a region of interest extending from the periosteal surface of the cortex to the tip of the last implant thread (yellow lines in Supplementary Figure 1B). BIC was defined as the length of implant surface within the region of interest in direct contact with bone (red lines in Supplementary Figure 1B). The percentage of peri-implant bone (highlighted in red in Supplementary Figure 1C) was calculated in a region of interest between the implant threads (highlighted in yellow in Supplementary Figure 1C). The bottom of the implant (green, Supplementary Figure 1B) was excluded from all calculations because pilot studies demonstrated variable

amounts of bone in this region (Supplementary Figure 1D), which is likely due to variations in placement of the implant into the marrow space.

**2.5.2 Biomechanical Analysis—**Biomechanical analyses were performed at the Cleveland Clinic Musculoskeletal Robotics and Mechanical Testing Core. Femurs were dissected and immediately transferred to phosphate buffered saline (PBS). Freshly harvested specimens were used to avoid potential artifacts due to fixation or freezing. Biomechanical pullout testing was performed using the Instron 5543 Frame (Instron, Norwood, MA) with a FlexTest SE Controller (MTS, Eden Prairie, MN). Force was measured through a 10 lb capacity load cell. Femurs were placed under wire loops embedded in PMMA, as illustrated in Supplementary Figure 2A. The implant was then gripped by a custom designed jig, which was then attached to the Instron Frame (Supplementary Figure 2A). The jig is composed of a base fixture and a top plate, shown in more detail in Supplementary Figure 2B. Pullout testing was performed at a displacement rate of 1 mm per minute. Ultimate force, stiffness and work to failure were determined from the resultant load versus displacement curves according to ASTM standards.

### 2.6 Statistical Analysis

All data passed normality (Kolmogorov-Smirnov test with Lilliefors' correction) and equal variance testing (Levene median test). Parametric One-Way ANOVA analyses were therefore performed followed by Bonferroni post-hoc tests (SigmaStat 3.0, Systat Software, San Jose, CA). A sample size of eight to thirteen mice per group was used for histomorphometric analysis and a sample size of seven to ten mice was used for biomechanical analysis. The specific sample size for each group is listed in the figure captions.

## 3. Results

### 3.1 Murine Model of Osseointegration - Qualitative Results

To develop a novel murine model of osseointegration, implants were autoclaved, as recommended by the manufacturer, and osseointegration was analyzed between 1 to 5 weeks following implantation. Observations of histological sections showed that during the 5 weeks following implantation there were increasing areas of bone in the marrow space surrounding the implant and directly in contact with the implant (white arrows in Figure 1A). Backscatter scanning electron microscopy images showed portions of the implant surface (white regions in Figure 2A) in direct contact with bone (grey regions in Figure 2A) without intervening soft tissue or cellular regions (black regions in Figure 2A). Bone-to-implant contact (BIC) was further confirmed by elemental analysis using x-ray energy dispersive spectroscopy, which verified the location of the implant, bone and marrow regions (Figure 2B). The location of the implant is shown by the elemental maps of titanium, aluminum and vanadium while the location of bone is shown by maps of calcium and phosphorus and the cellular marrow region is shown by a carbon map. The distribution of these regions can be best appreciated in the merged elemental map (Figure 2C). Histology, back-scatter scanning electron microscopy and μCT consistently demonstrated a greater amount of bone around the implant in the cross-sectional plane (Figure 1A, 2A, 2B, 3B) as compared to the longitudinal plane (Figure 1B & 1C). This is likely due to the implant being relatively close to cortical bone in all dimensions in the cross-sectional plane whereas in the longitudinal plane only the top and bottom of the implant are close to cortical bone.

Histology also demonstrated that a neo-cortex formed around the implant over the 5 week time course while the old cortex continually resorbed (Figure 1A). There was little bone formation at 1 week after insertion of the implant. However, at 2 and 3 weeks there was a

large amount of new bone (black arrows in Figure 1A) surrounding the old cortex (asterisks in Figure 1A). By 5 weeks, the old cortex was being resorbed and the neo-cortex was consolidating. This neo-cortex formation and remodeling was observed along a substantial length of the femur, which can be seen in both histology (brackets in left panels in Figure 1B) and μCT slices (Figure 1C). The increase in bone formation and remodeling seen in the implanted femur was local and not due to a systemic response as it did not occur in contralateral femurs (right panels in Figure 1B).

Osseointegration occurs through intramembraneous bone regeneration [46], which does not involve an intermediate cartilaginous phase. In contrast, endochrondral bone repair occurs during fracture healing in the absence of rigid fixation [47]. Consistent with intramembraneous osseointegration, cartilage was not observed around the implant at any time point in our model in sections stained with Toluidine Blue with acid etching (Figure 1A & 1B). To confirm the absence of cartilage, we performed Toluidine Blue staining on sections without acid etching. Eliminating acid etching impairs penetration of the stain into mineralized bone, thereby, selectively staining cartilaginous tissue [48]. Sections stained with Sanderson's Rapid Bone Stain were also examined for cartilage [45]. No cartilage was observed around the implant at any time point with either stain, confirming that bone repair in this model occurs intramembranously (Figure 3A & 3B, respectively). Femoral growth plates were used as positive controls and, as expected, stained purple with Toluidine Blue without etching and dark blue with Sanderson's Rapid Bone Stain. Thus, bone formation in our model occurs intramembraneously and is therefore similar to the bone formation that occurs in unicortical defects without implants [49].

### 3.2 Murine Model of Osseointegration - Quantitative Results

Examination of μCT scans revealed a halo artifact around the metal implant that makes it difficult to identify BIC (Figure 1C). Quantitative measurements of osseointegration were therefore restricted to histomorphometry and biomechanical pullout testing. Histomorphometric measurements were performed in the cross-sectional plane where a greater amount of bone was evident (see section 3.1). The percentage of BIC and the percentage of peri-implant bone (Figure 4A & 4B, respectively) increased significantly after 1 week following implantation ($p<0.001$ at 2, 3 and 5 weeks). The percentage of BIC continued to increase gradually from 2 to 5 weeks ($p=0.009$ at 5 weeks) while the percentage of peri-implant bone remained constant after 2 weeks. Biomechanical pullout testing parameters of ultimate force, stiffness and work to failure (Figure 4C, 4D & 4E, respectively) increased significantly between 1 and 2 weeks following implantation ($p<0.002$). Between 2 to 3 weeks, ultimate force remained constant (Figure 4C), stiffness increased (Figure 4D) and work to failure decreased (Figure 4E), although neither change was significant. Biomechanical analysis could not be performed at times longer than 3 weeks following implantation because bone growth around the neck of the implant prevented gripping of the implant to perform testing.

### 3.3 Surface Contaminants Inhibit Osseointegration

To test the hypothesis that removing contaminants from the surface of orthopaedic implants enhances osseointegration, we used the novel murine osseointegration model to compare the integration of implants that were autoclaved as recommended by the manufacturer and implants that underwent an additional rigorous cleaning procedure [30]. As expected, histomorphometric measurements of osseointegration in mice with the autoclaved implants (gray bars in Figure 5A & 5B) were similar to those found previously with autoclaved implants (Figure 4A & 4B). However, BIC was approximately two-fold higher ($p<0.001$) after 1 week with the rigorously cleaned implants (white bars in Figure 5A). This enhanced osseointegration was maintained at the 2 and 5 week time points ($p=0.001$ & $p<0.001$,

respectively). The increased BIC with the rigorously cleaned implants can be appreciated in the representative histological cross-sections shown in Figure 5C. For example, there is substantially more BIC with the rigorously cleaned implants than with the autoclaved implants (compare magnified panels in Figure 5C). In contrast, autoclaved and rigorously cleaned implants induced similar amounts of peri-implant bone formation (Figure 5B) and neo-cortex formation (compare Figure 5D and Figure 1B).

To more closely examine the effects of surface contaminants on osseointegration, we performed biomechanical pullout testing at the 1 week time point. For this purpose, we compared rigorously cleaned implants and two different lots of autoclaved implants that differed in their level of adherent LPS (Figure 6A). Rigorous cleaning of implants significantly increased biomechanical pullout measures of ultimate force ($p=0.005$), stiffness ($p<0.001$) and work to failure ($p=0.044$), compared to autoclaved implants (Figure 6B, 6C & 6D respectively). Interestingly, this increase in biomechanical parameters inversely correlated with levels of adherent LPS on these implants and all three biomechanical measures were approximately two fold higher for the rigorously cleaned implants than for the autoclaved implants with the highest levels of adherent LPS (Figure 6B, 6C & 6D).

## 4. Discussion

The two major goals of this study were to develop a murine model of osseointegration and to determine whether removing surface contaminants enhances osseointegration. The novel murine model of osseointegration is based on a previous established rat model [41,42]. Titanium alloy implants were implanted into a unicortical pilot hole in the mid-diaphysis of the femur and osseointegration was measured over a 5 week time course. Histology, backscatter scanning electron microscopy and x-ray energy dispersive spectroscopy showed areas of bone in intimate physical contact with the implant, confirming osseointegration. Histomorphometric measures of BIC and peri-implant bone and biomechanical measures of ultimate force, stiffness and work to failure increased significantly over time, also demonstrating successful osseointegration. This model was then used to determine whether removing contaminants, such as bacterial debris or manufacturing residues, remaining on orthopaedic implants after sterilization enhances osseointegration. We found that a rigorous cleaning procedure [30] significantly enhances osseointegration compared with implants that were autoclaved, as recommended by the manufacturer. The most likely interpretation of these results is that surface contaminants inhibit osseointegration.

Our murine model of osseointegration will provide two major benefits compared with current larger animal models [50]. First, it will allow the use of knock-out and transgenic mice to test the role of specific genes and molecular pathways in osseointegration. Second, it will allow for cost effective screening of potential countermeasures for impaired osseointegration prior to testing in larger animals. Two laboratories reported preliminary osseointegration studies in mice in the mid-1990s [51,52,53]. Recently, osseointegration studies in mice have demonstrated that molecular pathways known to regulate bone turnover also affect osseointegration. Colnot and colleagues used in situ hybridization to show that integration around titanium alloy implants involves molecular markers of bone remodeling [54]. Studies utilizing knock-out mice demonstrated that cyclooxygenase-2 and fibroblast growth factor receptor-3 play important roles in osseointegration [55,56]. Other investigators found that osseointegration is enhanced with local administration of retroviruses encoding osterix or by pre-coating titanium implants with fibronectin [27,57]. The performance of stainless steel and poly-lactide implants have also been examined in murine models [58,59]. However, osteoblasts do not form bone directly on these materials, which limits their usefulness in the study of osseointegration. Lastly, titanium ring implants were studied in murine calvaria [60]. However, this study was focused on vertical bone

growth around the ring implants, rather than integration. None of these previous studies examined clinically relevant implants or included biomechanical testing to fully characterize murine osseointegration. Biomechanical testing is necessary to evaluate the ability of an implant to sustain a load, an essential component of osseointegration. Our model includes a time course, appropriate sample size, quantitative analysis, clinically relevant implants and biomechanical testing. This is the first murine osseointegration study we know of that has included all of these parameters.

One limitation of our model is that it requires the use of young mice, since increased muscle size in older mice makes exposure of the femur prior to implantation extremely difficult without inducing extensive soft tissue damage. Young mice differ from older mice, most notably in their potential for bone regeneration [61]. In addition, mice have lower mechanical loads supporting their bones and a higher potential for bone regeneration than larger animals such as humans. The implant in our model is under non-loading conditions. However, non-loading models are useful to examine materials, coatings, or the effects of surface modifications on osseointegration before testing in a loading model [50]. Another limitation of our model is that because of the implant's small size, it is only possible to obtain one central histological section of the implant per mouse. Moreover, biomechanical testing can only be performed at time points up to 3 weeks following implantation because bone growth around the neck of the implant prevents gripping of the implant to perform testing. Despite these limitations, a murine model of osseointegration provides significant advantages as discussed in the previous paragraph and is appropriate for examining certain types of questions, such as whether surface contaminants inhibit osseointegration.

In our model, osseointegration occurs rapidly between 1 and 2 weeks (Figure 4), most likely because of the high potential for bone regeneration in young mice [61]. After 2 weeks, further osseointegration is modest, and bone remodeling is most likely occuring after this time point. Both histomorphometric and biomechanical measures increase in parallel (Figure 4), similar to the rat model of osseointegration described by Gabet and colleagues [41]. The forces that are measured by biomechanical pullout testing arise from the new bone in contact with the implant (BIC) as well as the bone in between the implant threads (peri-implant bone). Therefore, the three parameters of ultimate force, stiffness and work to failure that are generated from biomechanical testing, provide information about the mineralized tissue in the BIC and/or peri-implant bone [62]. Ultimate force is a measure of the failure of the mineralized tissue within the threads and is therefore dominated by the peri-implant bone. Stiffness is the immediate resistance of the mineralized tissue on the implant surface to deformation and is therefore dominated by the BIC. Work to failure is a measure of the energy that can be absorbed by the mineralized tissue and is the area under the force versus displacement curve. Therefore, work to failure is influenced by both the stiffness (BIC) and ultimate force (peri-implant bone)

We found that contaminants remaining on the implant surface after sterilization significantly inhibits osseointegration as assessed by measurements of BIC and biomechanical pullout testing (Figure 5 & 6). Autoclaved implants had higher levels of LPS, derived from Gram-negative bacteria, when compared to the rigorously cleaned implants that have enhanced osseointegration. Because soluble LPS inhibits osteoblast cell differentiation on tissue culture plastic [63,64,65], it is likely that adherent LPS on the surface of implants can inhibit osteoblast differentiation and thereby inhibit osseointegration. Our results do not however demonstrate that adherent LPS caused the impaired osseointegration since we can not exclude the possibility that other contaminants on the autoclaved implants may also impair osseointegration.

In this study, surface contaminants inhibited BIC and biomechanical pullout testing without affecting either peri-implant bone or the neo-cortex formation (Figure 5 & 6). These results are reminiscent of the finding that surface roughness enhanced BIC and biomechanical parameters in a rabbit osseointegration model but had no affect on peri-implant bone formation [23]. Thus, both surface contaminants and surface topography primarily effect bone formation on the implant surface (BIC) and have less effect on more distant bone formation (peri-implant bone). In contrast, we would predict that stimulation of bone formation in general would increase both BIC and peri-implant bone as has been shown with systemic parathyroid hormone (PTH) treatment [42]. In the PTH study, biomechanical pullout testing results primarily correlated with the amount of peri-implant bone formation rather than with BIC as we observed. This is likely due to the different spatial pattern of effects induced by implant surface modifications and systemic treatments.

In this study we developed a novel osseointegration model that provides quantitative and reproducible measurements of osseointegration in mice. Using this model, we found that contaminants on orthopaedic implants inhibit osseointegration as measured by histomorphometry and biomechanical pullout testing. The results of this study justify the need for the development of better detection and removal techniques for contaminants on orthopaedic implants and other medical devices.

Highlights

- Developed a novel murine model of ossointegration
- Osseointegration characterized by histomorphometry, back-scatter SEM, XEDS, and biomechanical pullout testing
- Surface contaminants inhibited bone-to-implant contact and biomechanical pullout testing

## Supplementary Material

Refer to Web version on PubMed Central for supplementary material.

## Acknowledgments

This work was supported by NIH T32 AR07505 (LAB), a pilot grant from the CCF/NIH Musculoskeletal Core Center Grant P30 AR-050953 (EMG & RWC), a Sulzer Medical Research Fund Grant (EMG & VMG), and the Harry E. Figgie III MD Professorship (EMG). We would like to thank Reza Sharghi-Moshtahgin for assistance with backscatter scanning electron microscopy and x-ray energy dispersive spectroscopy; Radhika Patel and Antoine van den Bogert for their help with biomechanical testing; Teresa Pizzuto for histological preparation; and Amit Vasanji for μCT assistance.

## References

1. Kurtz S, Ong K, Lau E, Mowat F, Halpern M. Projections of primary and revision hip and knee arthroplasty in the United States from 2005 to 2030. J Bone Joint Surg Am. 2007; 89:780–785. [PubMed: 17403800]
2. Sundfeldt M, Carlsson L, Johansson C, Thomsen P, Gretzer C. Aseptic loosening, not only a question of wear: a review of different theories. Acta Orthop. 2006; 77:177–197. [PubMed: 16752278]
3. Holt G, Murnaghan C, Reilly J, Meek RM. The biology of aseptic osteolysis. Clin Orthop Relat Res. 2007; 460:240–252. [PubMed: 17620815]
4. Jain NB, Higgins LD, Ozumba D, Guller U, Cronin M, Pietrobon R, Katz JN. Trends in epidemiology of knee arthroplasty in the United States, 1990–2000. Arthritis Rheum. 2005; 52:3928–3933. [PubMed: 16320340]

5. Khatod M, Inacio M, Paxton EW, Bini SA, Namba RS, Burchette RJ, Fithian DC. Knee replacement: epidemiology, outcomes, and trends in Southern California: 17,080 replacements from 1995 through 2004. Acta Orthop. 2008; 79:812–819. [PubMed: 19085500]
6. Bauer TW, Schils J. The pathology of total joint arthroplasty.II. Mechanisms of implant failure. Skeletal Radiol. 1999; 28:483–497. [PubMed: 10525792]
7. Albrektsson T, Branemark P, Hansson H, Lindstrom J. Osseointegrated titanium implants. Requirements for ensuring a long-lasting, direct bone-to-implant anchorage in man. Acta Orthopaedica Scandinavica. 1981; 52:155–170. [PubMed: 7246093]
8. Branemark R, Branemark P, Rydevik B, Myers R. Osseointegration in skeletal reconstruction and rehabilitation: a review. J. Rehabil. Res. Dev. 2001; 38:175–181. [PubMed: 11392650]
9. Puleo DA, Nanci A. Understanding and controlling the bone-implant interface. Biomaterials. 1999; 20:2311–2321. [PubMed: 10614937]
10. Ozawa S, Ogawa T, Iida K, Sukotjo C, Hasegawa H, Nishimura R, Nishimura I. Ovariectomy hinders the early stage of bone-implant integration: histomorphometric, biomechanical, and molecular analyses. Bone. 2002; 30:137–143. [PubMed: 11792576]
11. Mellado-Valero A, Ferrer-Garcia J, Herrera-Ballester A, Labaig-Rueda C. Effects of diabetes on the osseointegration of dental implants. Med. Oral. Patol. Oral Cir. Bucal. 2007; 12:E38–E43. [PubMed: 17195826]
12. Sakakura C, Margonar R, Holzhausen M, Nociti F, Alba R, Marcantonio E. Influence of cyclosporin A therapy on bone healing around titanium implants: a histometric and biomechanic study in rabbits. J. Periodontol. 2003; 74:976–981. [PubMed: 12931759]
13. Cesar-Neto J, Duarte P, Sallum E, Barbieri D, Moreno H, Nociti F. A comparative study on the effect of nicotine administration and cigarette smoke inhalation on bone healing around titanium implants. J. Periodontol. 2003; 74:1454–1459. [PubMed: 14653391]
14. Meldrum R, Wurtz L, Feinberg J, Capello W. Does smoking affect implant survivorship in total hip arthroplasty? A preliminary retrospective case series. Iowa Orthop. J. 2005; 25:17–24. [PubMed: 16089066]
15. Bechtold J, Kubic V, Soballe K. A controlled experimental model of revision implants: Part I. Development. Acta Orthopaedica Scandinavica. 2001; 72:642–649. [PubMed: 11817882]
16. Bechtold J, Mouzin O, Kidder L, Soballe K. A controlled experimental model of revision implants: Part II. Implementation with loaded titanium implants and bone graft. Acta Orthopaedica Scandinavica. 2001; 72:650–656. [PubMed: 11817883]
17. Aspenberg P, Herbertsson P. Periprosthetic bone resorption. Particles versus movement. J Bone Joint Surg Br. 1996; 78:641–646. [PubMed: 8682835]
18. Ryd L, Albrektsson B, Carlsson L, Dansgard F, Herberts P, Lindstrand A, Regner L, Toksvig-Larsen S. Roentgen stereophotogrammetric analysis as a predictor of mechanical loosening of knee prostheses. Journal of Bone and Joint Surgery. 1995; 77B:377–383.
19. Schmalzried T, Jasty M, Harris W. Periprosthetic bone loss in total hip arthroplasty. Polyethylene wear debris and the concept of the effective joint space. Journal of Bone and Joint Surgery. 1992; 74A:849–863. [PubMed: 1634575]
20. Dean JC, Tisdel CL, Goldberg VM, Parr J, Davy D, Stevenson S. Effects of hydroxyapatite tricalcium phosphate coating and intracancellous placement on bone ingrowth in titanium fibermetal implants. J Arthroplasty. 1995; 10:830–838. [PubMed: 8749769]
21. Wataha JC. Materials for endosseous dental implants. J Oral Rehabil. 1996; 23:79–90. [PubMed: 8850057]
22. Goldberg VM, Stevenson S, Feighan J, Davy D. Biology of grit-blasted titanium alloy implants. Clin Orthop Relat Res. 1995:122–129. [PubMed: 7554621]
23. Feighan JE, Goldberg VM, Davy D, Parr JA, Stevenson S. The influence of surface-blasting on the incorporation of titanium-alloy implants in a rabbit intramedullary model. J Bone Joint Surg Am. 1995; 77:1380–1395. [PubMed: 7673290]
24. Giavaresi G, Fini M, Chiesa R, Rimondini L, Rondelli G, Borsari V, Martini L, Nicolialdini N, Guzzardella GA, Giardino R. Osseointegration of sandblasted or anodised hydrothermally-treated titanium implants: mechanical, histomorphometric and bone hardness measurements. Int J Artif Organs. 2002; 25:806–813. [PubMed: 12296466]

25. Schwarz ML, Kowarsch M, Rose S, Becker K, Lenz T, Jani L. Effect of surface roughness, porosity, and a resorbable calcium phosphate coating on osseointegration of titanium in a minipig model. J Biomed Mater Res A. 2008
26. Degasne I, Basle MF, Demais V, Hure G, Lesourd M, Grolleau B, Mercier L, Chappard D. Effects of roughness, fibronectin and vitronectin on attachment, spreading, and proliferation of human osteoblast-like cells (Saos-2) on titanium surfaces. Calcif Tissue Int. 1999; 64:499–507. [PubMed: 10341022]
27. Jimbo R, Sawase T, Shibata Y, Hirata K, Hishikawa Y, Tanaka Y, Bessho K, Ikeda T, Atsuta M. Enhanced osseointegration by the chemotactic activity of plasma fibronectin for cellular fibronectin positive cells. Biomaterials. 2007; 28:3469–3477. [PubMed: 17512051]
28. Sousa SR, Lamghari M, Sampaio P, Moradas-Ferreira P, Barbosa MA. Osteoblast adhesion and morphology on TiO2 depends on the competitive preadsorption of albumin and fibronectin. J Biomed Mater Res A. 2008; 84:281–290. [PubMed: 17607748]
29. Spiegelberg, S. ASTM Activities for Assessing Cleanliness of Medical Devices. Shrivastava, S., editor. Materials Park: Medical Device Materials, ASM International; 2004. p. 125-126.
30. Ragab AA, VanDeMotter R, Lavish SA, Goldberg VM, Ninomiya JT, Carlin CR, Greenfield EM. Measurement and removal of adherent endotoxin from titanium particles and implant surfaces. Journal of Orthopaedic Research. 1999; 17:803–809. [PubMed: 10632445]
31. Magalhaes PO, Lopes AM, Mazzola PG, Rangel-Yagui C, Penna TC, Pessoa A Jr. Methods of endotoxin removal from biological preparations: a review. J Pharm Pharm Sci. 2007; 10:388–404. [PubMed: 17727802]
32. Ross VC, Twohy CW. Endotoxins and medical devices. Prog Clin Biol Res. 1985; 189:267–281. [PubMed: 4048209]
33. Nelson SK, Knoernschild KL, Robinson FG, Schuster GS. Lipopolysaccharide affinity for titanium implant biomaterials. J Prosthet Dent. 1997; 77:76–82. [PubMed: 9029469]
34. Lee MS, Kim YJ. Signaling pathways downstream of pattern-recognition receptors and their cross talk. Annu Rev Biochem. 2007; 76:447–480. [PubMed: 17328678]
35. Zahringer U, Lindner B, Inamura S, Heine H, Alexander C. TLR2 - promiscuous or specific? A critical re-evaluation of a receptor expressing apparent broad specificity. Immunobiology. 2008; 213:205–224. [PubMed: 18406368]
36. US Department of health and human services/Public Health services/Food and Drug Administration. Guideline on validation of the limulus amebocyte lysate test as an end-product endotoxin test for human and animal parenteral drugs, biological products, and medical devices. 1987. p. 1-30.
37. Arys A, Philippart C, Dourov N, He Y, Le QT, Pireaux JJ. Analysis of titanium dental implants after failure of osseointegration: combined histological, electron microscopy, and X-ray photoelectron spectroscopy approach. J Biomed Mater Res. 1998; 43:300–312. [PubMed: 9730068]
38. Daniel, A.; Kimmelman, E. The FDA and Worldwide Quality System Requirements Guidebook for Medical Devices. 2nd ed.. Milwaukee: ASQ Quality Press; 2008.
39. Spiegelberg, S. How Clean is Clean Enough?. San Antonio: ASTM Workshop of Medical Device Cleanliness; 2010.
40. Bethesda: 2003. Orthopaedic Device Forum Meeting Summation Report.
41. Gabet Y, Muller R, Levy J, Dimarchi R, Chorev M, Bab I, Kohavi D. Parathyroid hormone 1–34 enhances titanium implant anchorage in low-density trabecular bone: a correlative micro-computed tomographic and biomechanical analysis. Bone. 2006; 39:276–282. [PubMed: 16617039]
42. Gabet Y, Kohavi D, Voide R, Mueller TL, Muller R, Bab I. Endosseous implant anchorage is critically dependent on mechanostructural determinants of peri-implant bone trabeculae. J Bone Miner Res. 2010; 25:575–583. [PubMed: 19653813]
43. Nalepka JL, Greenfield EM. Detection of bacterial endotoxin in human tissues. Biotechniques. 2004; 37:413–417. [PubMed: 15470896]

44. Bloebaum R, Willie B, Mitchell B, Hofmann A. Relationship between bone ingrowth, mineral apposition rate, and osteoblast activity. Journal of Biomedical Materials Research. 2007; 81A: 505–514. [PubMed: 17236212]
45. Wang ML, Massie J, Allen RT, Lee YP, Kim CW. Altered bioreactivity and limited osteoconductivity of calcium sulfate-based bone cements in the osteoporotic rat spine. Spine J. 2008; 8:340–350. [PubMed: 17983844]
46. Jasty, M.; Kienapfel, H.; Griss, P. Fixation by Ingrowth. In: Callaghan, J.; Rosenberg, A.; Rubash, H., editors. The Adult Hip. Lippincott Williams and Wilkins: Philadelphia; 2007. p. 195-203.
47. Thompson Z, Miclau T, Hu D, Helms JA. A model for intramembranous ossification during fracture healing. J Orthop Res. 2002; 20:1091–1098. [PubMed: 12382977]
48. Dickson, G. Methods of Calcified Tissue Preparation. New York: Elsevier; 1984.
49. Lu C, Huang S, Miclau T, Helms JA, Colnot C. Mepe is expressed during skeletal development and regeneration. Histochem Cell Biol. 2004; 121:493–499. [PubMed: 15221418]
50. Sumner D, Turner T, Urban R. Animal models relevant to cementless joint replacement. J. Musculoskelet. Neuronal Interact. 2001; 1:333–345. [PubMed: 15758484]
51. Rahal MD, Branemark PI, Osmond DG. Response of bone marrow to titanium implants: osseointegration and the establishment of a bone marrow-titanium interface in mice. Int. J. Oral Maxillofac. Implants. 1993; 8:573–579. [PubMed: 8112799]
52. Morberg P, Isaksson O, Johansson C, Sandstedt J, Tornell J. Improved early bone-implant integration in transgenic mice overexpressing bovine growth hormone. J. Mat. Sci.:Materials in Medicine. 1995; 6:541–544.
53. Morberg P, Isaksson O, Johansson C, Sandstedt J, Tornell J. Improved long-term bone-implant integration. Experiments in transgenic mice overexpressing bovine growth hormone. Acta Orthopaedica Scandinavica. 1997; 68:344–348. [PubMed: 9310037]
54. Colnot C, Romero DM, Huang S, Rahman J, Currey JA, Nanci A, Brunski JB, Helms JA. Molecular analysis of healing at a bone-implant interface. J Dent Res. 2007; 86:862–867. [PubMed: 17720856]
55. Chikazu D, Tomizuka K, Ogasawara T, Saijo H, Koizumi T, Mori Y, Yonehara Y, Susami T, Takato T. Cyclooxygenase-2 activity is essential for the osseointegration of dental implants. Int J Oral Maxillofac Surg. 2007; 36:441–446. [PubMed: 17376655]
56. Letitia L HA, Li A, Wang H, Li W, Harvey E, Henderson J. A Murine Model of Osetoarthritis: Impact on Osseointegration. Trans Orthop Res Soc. 2008; 33:1875.
57. Xu B, Zhang J, Brewer E, Tu Q, Yu L, Tang J, Krebsbach P, Wieland M, Chen J. Osterix enhances BMSC-associated osseointegration of implants. J Dent Res. 2009; 88:1003–1007. [PubMed: 19828887]
58. Leucht P, Kim JB, Wazen R, Currey JA, Nanci A, Brunski JB, Helms JA. Effect of mechanical stimuli on skeletal regeneration around implants. Bone. 2007; 40:919–930. [PubMed: 17175211]
59. Popelut A, Rooker SM, Leucht P, Medio M, Brunski JB, Helms JA. The acceleration of implant osseointegration by liposomal Wnt3a. Biomaterials. 2010; 31:9173–9181. [PubMed: 20864159]
60. Freilich M, C MP, Wei M, Shafer D, Schleier P, Hortschansky P, Kompali R, Kuhn L. Growth of new bone guided by implants in a murine calvarial model. Bone. 2008; 43:781–788. [PubMed: 18589010]
61. Wahl EC, Aronson J, Liu L, Fowlkes JL, Thrailkill KM, Bunn RC, Skinner RA, Miller MJ, Cockrell GE, Clark LM, Ou Y, Isales CM, Badger TM, Ronis MJ, Sims J, Lumpkin CK Jr. Restoration of regenerative osteoblastogenesis in aged mice: modulation of TNF. J Bone Miner Res. 2010; 25:114–123. [PubMed: 19580462]
62. Berzins, A.; Sumner, D. Implant Pushout and Pullout Test. In: An, Y.; Draughn, R., editors. Mechanical Testing of Bone and the Bone-Implant Interface. Boca Raton: CRC Press LLC; 2000. p. 463-476.
63. Loomer PM, Ellen RP, Tenenbaum HC. Characterization of inhibitory effects of suspected periodontopathogen on osteogenesis in vitro. Infect. Immun. 1995; 63:3287–3296. [PubMed: 7642257]

64. Kadono H, Kido J, Kataoka M, Yamauchi N, Nagata T. Inhibition of osteoblastic cell differentiation by lipopolysaccharide extract from Porphyromonas gingivalis. Infect. Immun. 1999; 67:2841–2846. [PubMed: 10338489]

65. Xing Q, Ye Q, Fan M, Zhou Y, Xu Q, Sandham A. Porphyromonas gingivalis lipopolysaccharide inhibits the osteoblastic differentiation of preosteoblasts by activating Notch1 signaling. J Cell Physiol. 2010; 225:106–114. [PubMed: 20648628]

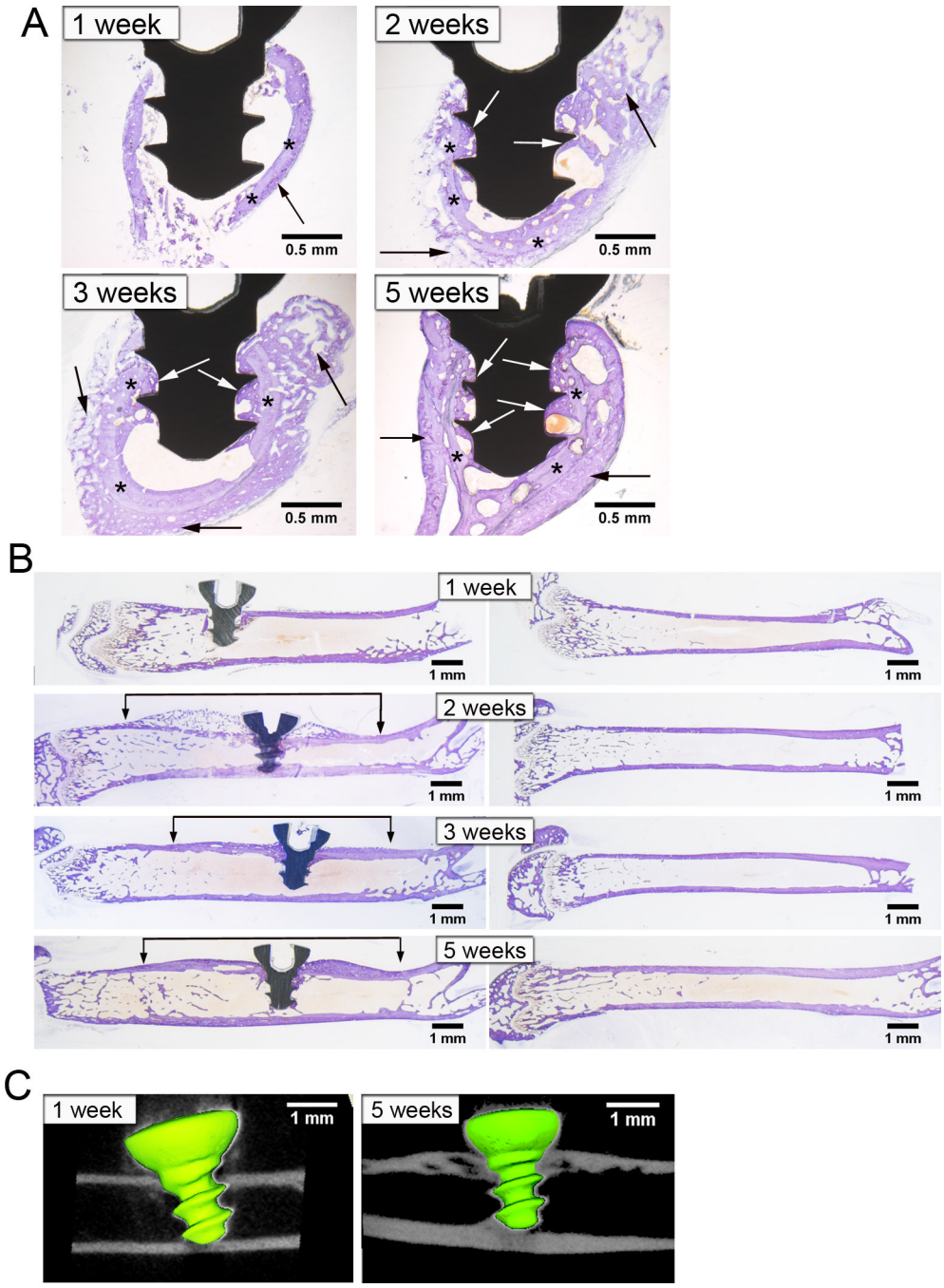


**Figure 1. Histological and µCT Analysis of Osseointegration**

Cross-sections (A) and longitudinal sections (B) stained with Toluidine Blue after acid etching at 1, 2, 3 and 5 weeks after implantation. Old bone is indicated by lighter purple staining while new bone is indicated by darker purple staining. Black arrows indicate bone formation surrounding the old cortex, which is indicated by asterisks. White arrows indicate new bone that is around and in contact with the implant. Brackets indicate bone formation and remodeling along length of femur. µCT Longitudinal slices at 1 and 5 weeks after implantation (C). Note halo artifact around the implant. Representative images of n=9–10 in (A) and n=2–3 in (B).

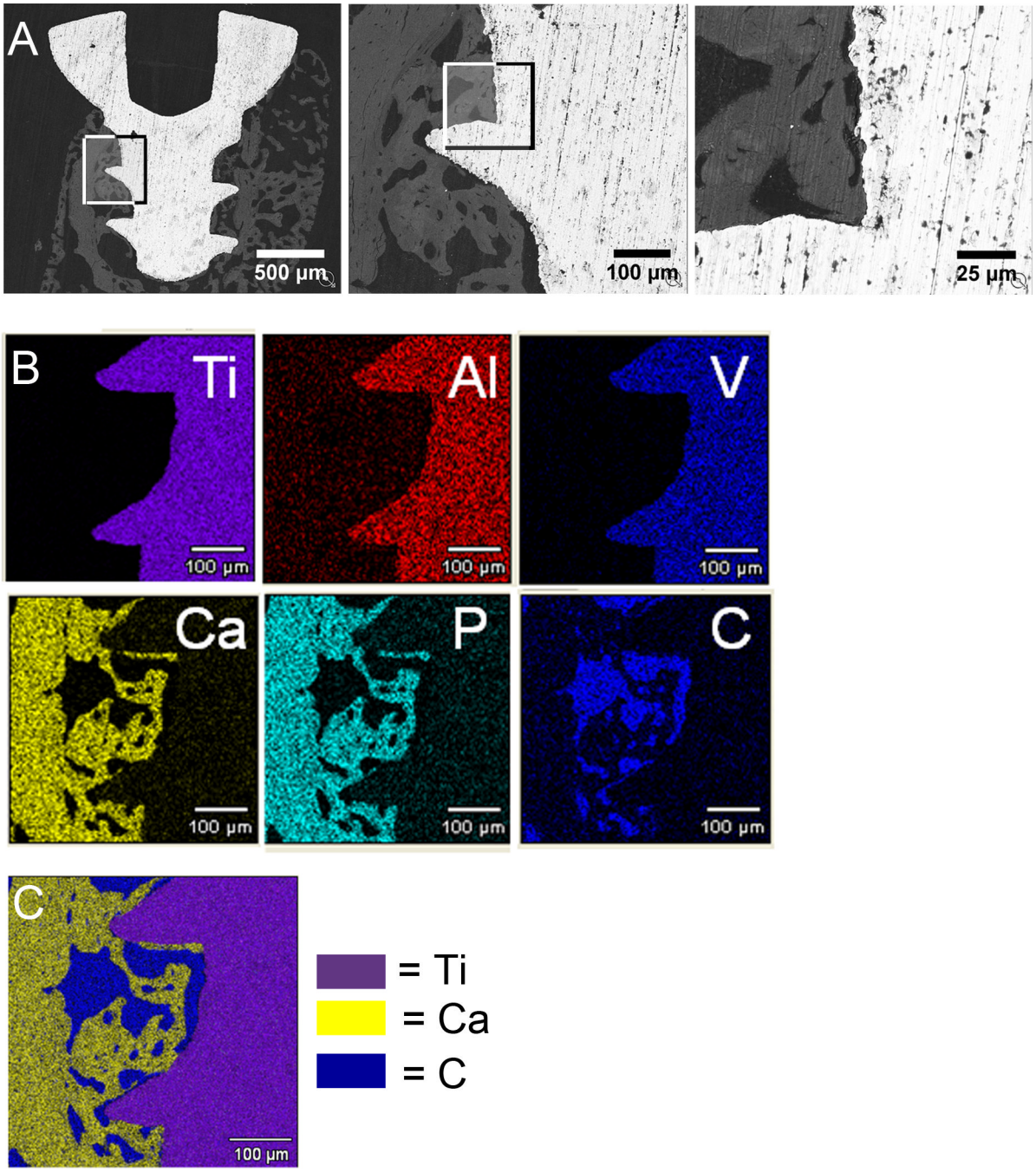


**Figure 2. Backscatter Scanning Electron Microscopic Analysis of Osseointegration**

Images at 2 weeks after implantation: bone (white), implant (grey) and marrow cells (black) (A). Boxes indicate areas magnified in next panel. Elemental analysis using x-ray energy dispersive spectroscopy at 2 weeks after implantation (B). Elemental maps of titanium (purple), aluminum (red) and vanadium (blue) are shown in the top panel. Elemental maps of calcium (yellow), phosphorous (aqua) and carbon (blue) are shown in the bottom panel. Merged image of elemental analysis showing titanium, calcium and carbon (C). Similar results were obtained at 5 weeks following implantation. Representative images of n=2.

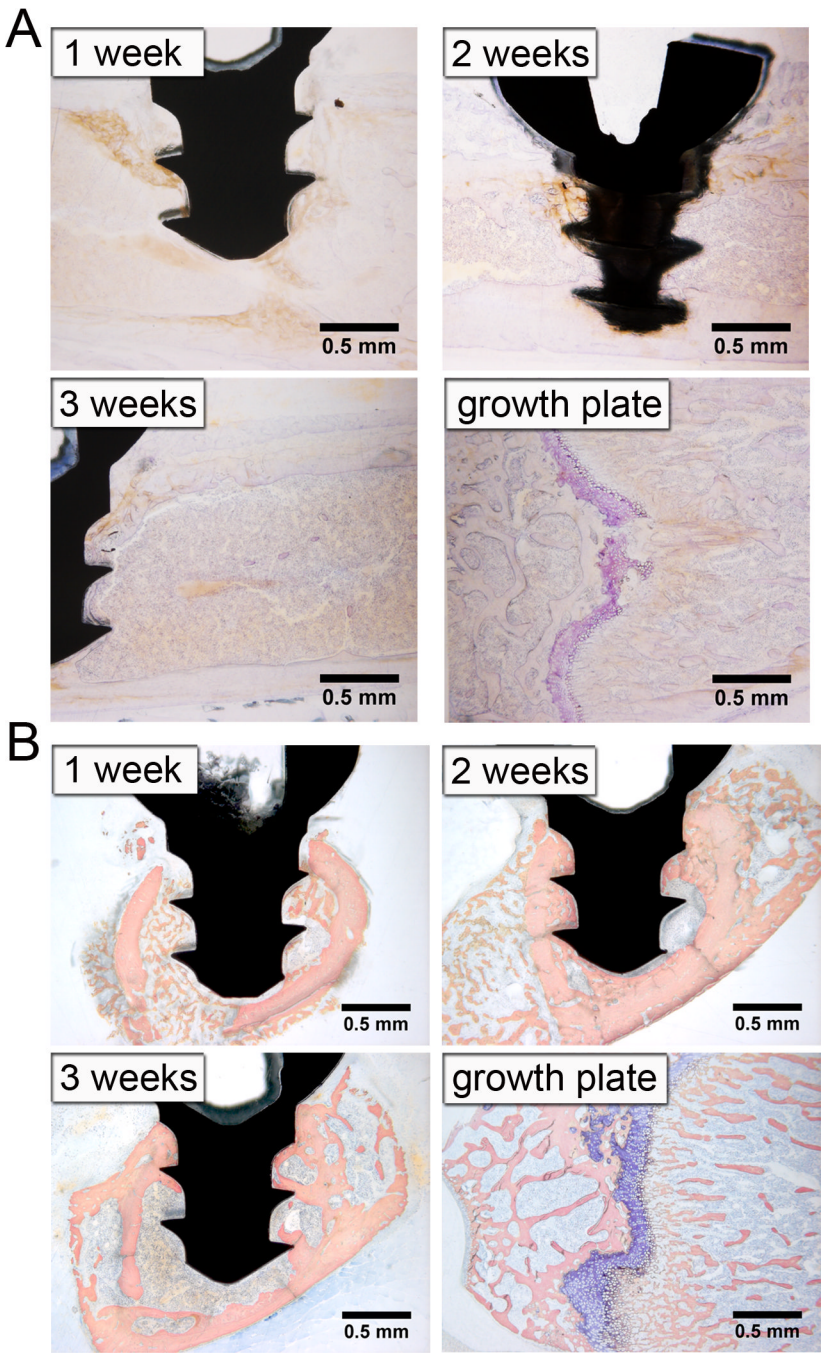


**Figure 3. Bone Formation and Remodeling is Intramembraneous**

Longitudinal sections stained with Toluidine blue without acid etching at 1, 2, and 3 weeks after implantation (A). Purple staining indicates cartilage at growth plate. Cross-sections stained with Sanderson's Rapid Bone Stain at 1, 2 and 3 weeks following implantation (B). Mineralized bone is indicated by pink staining, marrow cells by light blue staining, and cartilage by dark blue staining. Note lack of cartilage around implant. Representative images of n=2–3 in (A) and n=9–10 in (B).

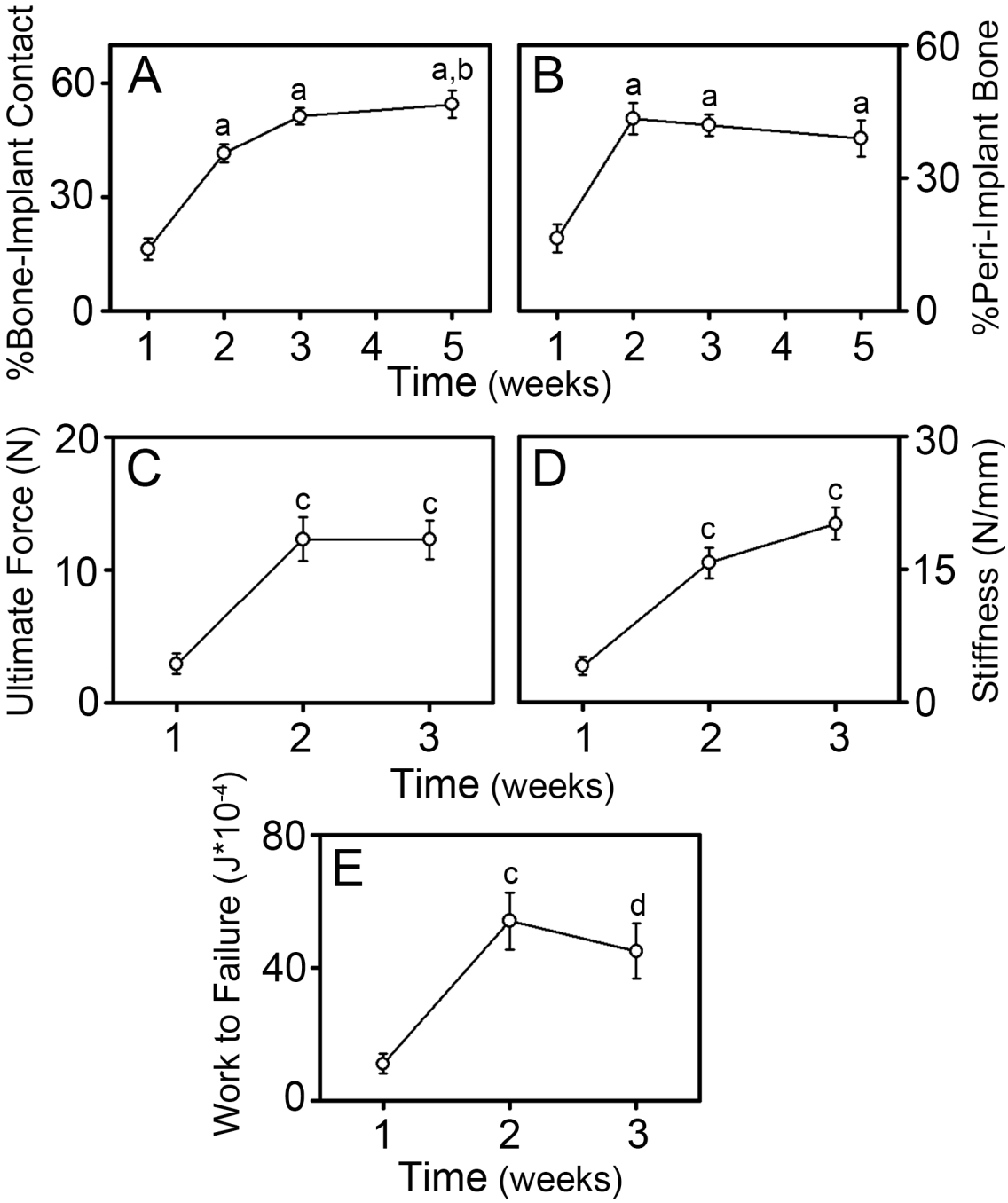


**Figure 4. Histomorphometric and Biomechanical Analysis of Osseointegration**

Histomorphometric measures of the percentage of bone to implant contact (BIC) (A) and the percentage of peri-implant bone (B). Pullout testing parameters of ultimate force (C), stiffness (D), and work to failure (E). Data shown as mean ± SEM; "a" denotes $p<0.001$ compared to 1 week, "b" denotes $p=0.009$ compared to 2 weeks, "c" denotes $p<0.002$ compared to 1 week, and "d" denotes $p=0.006$ compared to 1 week. For histomorphometric analysis, n=8 at 1 week, n=13 at 2 and 3 weeks, and n=10 at 5 weeks. For biomechanical analysis, n=9 at 1 week, n=8 at 2 weeks, and n=10 at 3 weeks.

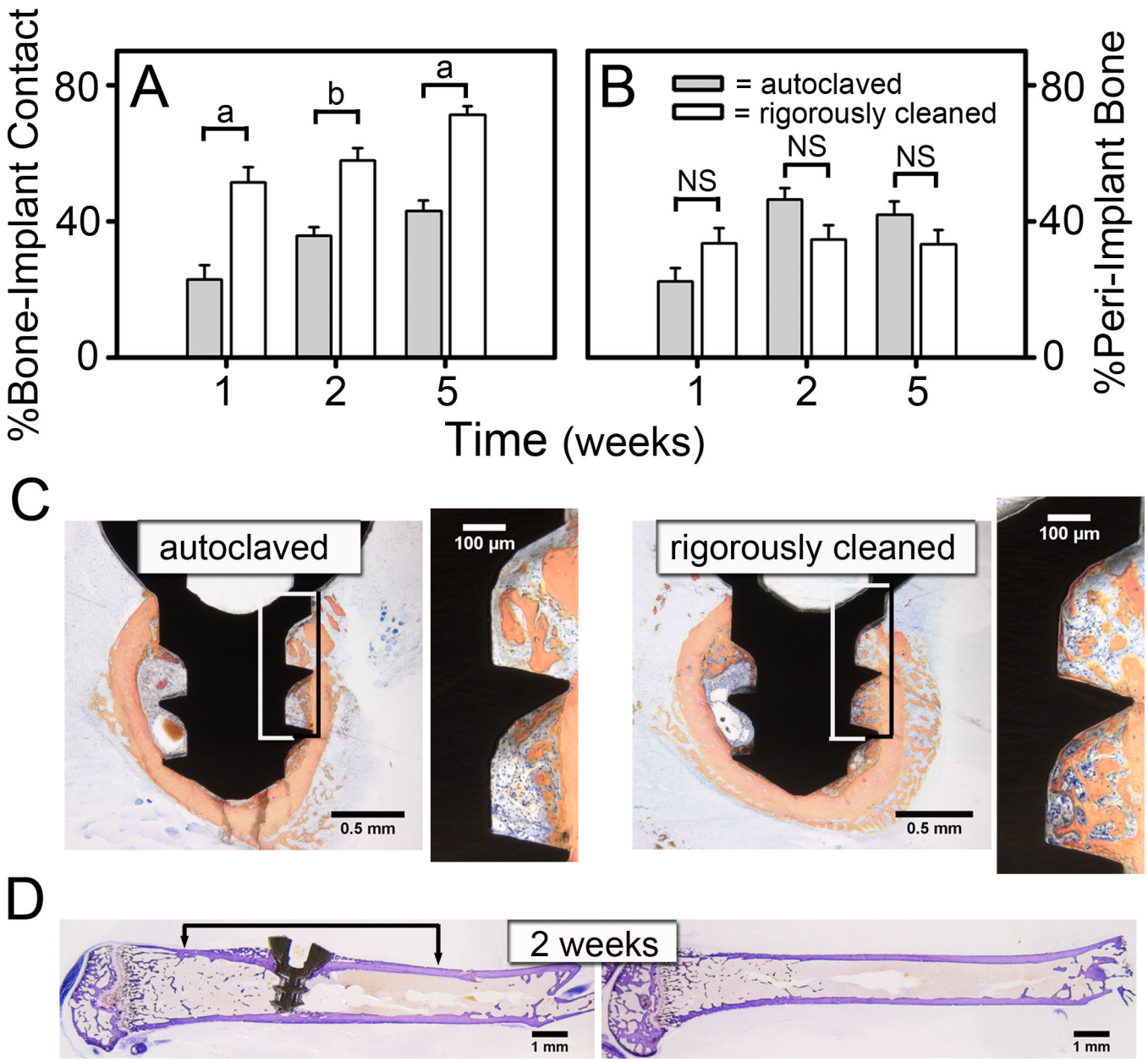


**Figure 5. Rigorous Cleaning of Implants Enhances Bone to Implant Contact**

Histomorphometric measures of the percentage of BIC (A) and the percentage of peri-implant bone (B). Representative histological cross-sections of rigorously cleaned and autoclaved implants at 1 week following implantation (C). Boxes indicate areas magnified in next panel. Representative longitudinal histological sections of rigorously cleaned implants at 2 weeks after implantation (D). Data shown as mean ± SEM; “a” denotes $p<0.001$ and “b” denotes $p=0.001$. For rigorously cleaned implants, n=9 at 1 week, n=8 at 2 weeks and n=10 at 5 weeks. For autoclaved implants, n=10 at 1 & 5 weeks and n=9 at 2 weeks.

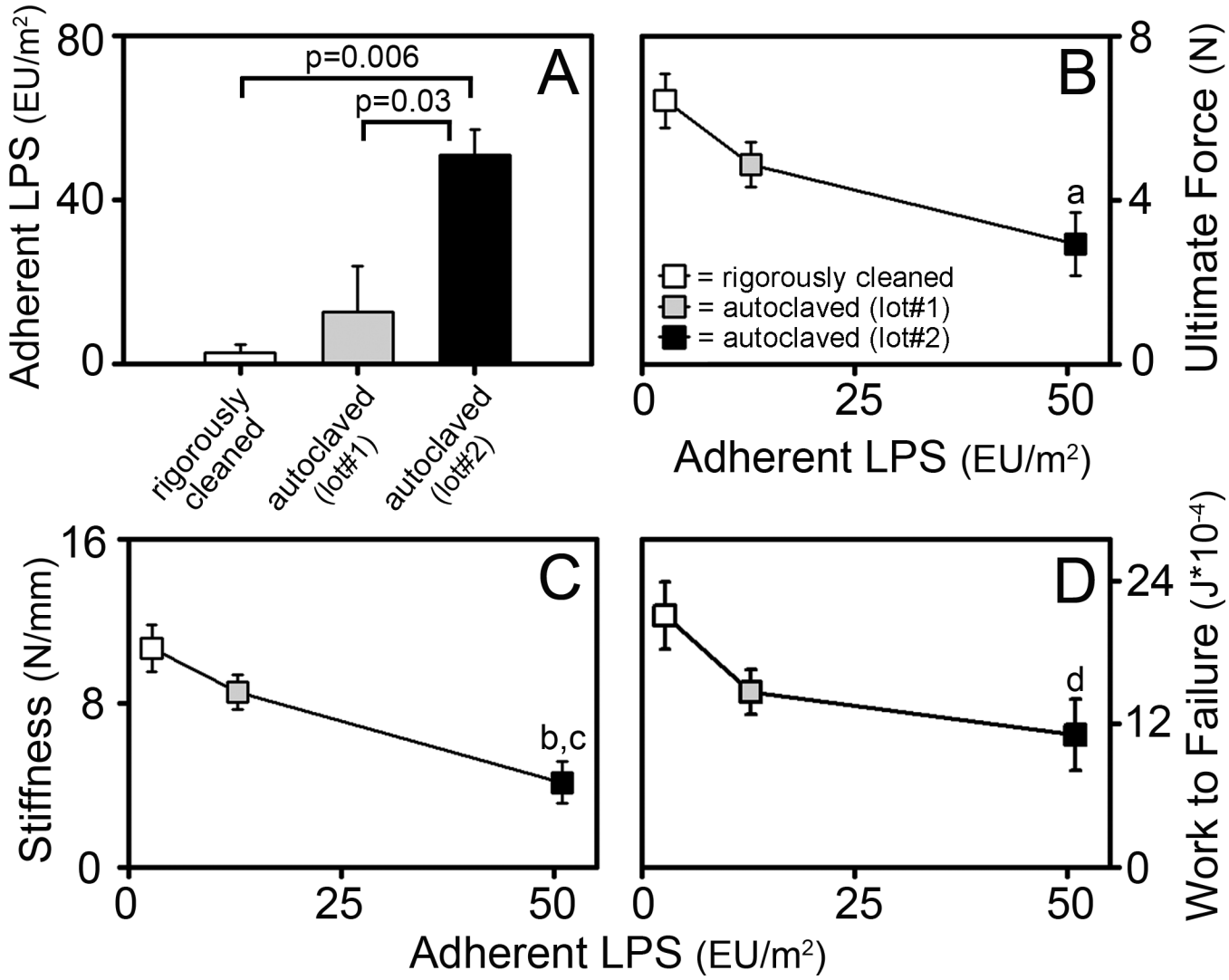


**Figure 6. Rigorous Cleaning of Implants Enhances Biomechanical Measures of Osseointegration**

Adherent LPS on rigorously cleaned implants and two lots of autoclaved implants (A). Pullout testing parameters at 1 week after implantation of ultimate force (B), stiffness (C), and work to failure (D) vs. adherent LPS. Rigorously cleaned implants (white bar in A and white symbols in B–D) were prepared from the same lot of implants as autoclaved lot#1 (grey bar in A and grey symbols in B–D). Autoclaved lot #2 (black bar in A and black symbols in B–D) are from the same lot of implants shown in Figure 5C–E. Data shown as mean ± SEM; “a” denotes p=0.005, “b” denotes p<0.001 and “d” denotes p=0.044 compared to rigorously cleaned implants; “c” denotes p=0.014 compared to autoclaved lot#1. For rigorously cleaned implants, n=7. For autoclaved implants lot #1, n=8. For autoclaved implants lot#2, n=9.